Progress In Electromagnetics Research B, Vol. 70, 113–130, 2016

Analytical Electromagnetic Analysis of Multi-Phases Cage Rotor Induction Motors in Healthy, Broken Bars and Open Phases Conditions

Lazhar Roubache*, Kamel Boughrara, and Rachid Ibtiouen

Abstract—This paper presents an analytical calculation of magnetic field and electromagnetic performances of 3-, 5-, 7-, 9-, 11-phases cage rotor induction machines in healthy, broken bars and open phase's conditions. This model is formulated to consider all types of multi-phase/multipoles windings and used for the identification of electrical equivalent circuit (EEC) parameters It's based on the subdomain model and the resolution of Poisson's, Laplace's, and Helmholtz's equations in each subdomain issued from Maxwell equations using the method of separation of variables and Fourier series when the machines are fed with sinusoidal current and voltage. The developed analytical model permits the calculation of magnetic field distribution, eddy current, circuit model parameters, and unbalanced magnetic radial force due to broken bars, electromagnetic torque and absorbed stator current. A comparative analysis between the studied five multi-phases machines is done with considering identical power rate. The analytical results are validated by those issued from the finite-element method (FEM).

1. INTRODUCTION

Polyphase cage rotor induction motors have many advantages, thanks to their easy and robust construction. This type of machine is being extensively used in several applications [1–3]. In the literature many multi-phases machine topics have been addressed, such as multi-phase machine advantages, properties, modeling, and performance with different control techniques [2–5]. One further advantage is that multi-phase machines are said to be fault-tolerant, offering greater security in mission-critical applications [5].

The designs and developments of multi-phase induction machines depend on the existing computer-aided analytical design tool. It's possible to use numerical methods (i.e., finite elements or the finite differences) [3, 6, 7] to analysis the electromagnetic performances of multi-phase induction machines, and their react against fault in rotor bars or in ones of their phases. However these approaches are time consuming and not suitable for the optimization problems. Some of recent 2-D static analytical predictions of magnetic field distribution are proposed in [8–12]. The model presented in [8] which takes into account rotor and stator semi-slots gives good results in the calculation of magnetic field, eddy-currents, EEC parameters, and steady-state performances of three phase's induction motors in healthy and broken bar conditions.

In this paper, we generalize this model for n-phases cage rotor induction motors without rotor and stator semi-slots in healthy case, broken bars and open phase's conditions, and use it for analysis of 3-, 5-, 7-, 9-, 11-phases identical power rated multi-phase machines. To facilitate the evaluation of various stator designs, the same phase current as well as flux per pole is used in all machines.

Received 25 July 2016, Accepted 11 October 2016, Scheduled 30 October 2016
* Corresponding author: Lazhar Roubache (roubache.lazhar@gmail.com).
The authors are with the Ecole Nationale Polytechnique (LRE-ENP), Algiers, 10, Av. Pasteur, El Harrach, BP 182, 16200, Algeria.

The contributions of this paper are divided among the various sections. Section 2 includes the machine design and specifications, and the differential equations to be solved in each part of the machine. Section 3 presents the analytical solutions of Laplace's, Poisson's, and Helmholtz's equations. Section 4 shows the identification of the EEC of the multi-phases machine parameters and the calculation of radial force in the air gap created in broken bars condition. It is noticed that the radial force is null for open phases condition. Symmetry of magnetic flux lines is also realized in this case. Results and validation of the analytic model with FEM [14], and comparative study between the n-phase machines designed is given in Sections 5 and 6. Finally, the conclusion in Section 7.

2. PROBLEM DEFINITIONS

In this paper, a subdomain analytical model based on Maxwell equations is applied to analyze the electromagnetic performances of 3-, 5-, 7-, 9-, and 11-phases machines in healthy and fault conditions and fed with current and voltage. The stator winding of the studied machines is distributed in slots with integer number of slot per pole and per phase. The five machines have the same output power, to get a comparative study and in the same time validate the analytical multi-phase model.

2.1. Machines Design

In this section, a low-voltage three-phase machine is used as reference for comparison with other multi-phase machines. Fig. 1 shows the machine model where Region I represents the air-gap, Region II the rotor bars, Regions III the stator slots.

Using principles of the design in [13], the other multi-phase machines are designed to accommodate the constant volume rotors and obtain the same output power and phase current level. Hence, over the parameters given in the following equations, all the other parameters are the same for all machines, the five designed machines and their corresponding parameters are shown in the Table 1.

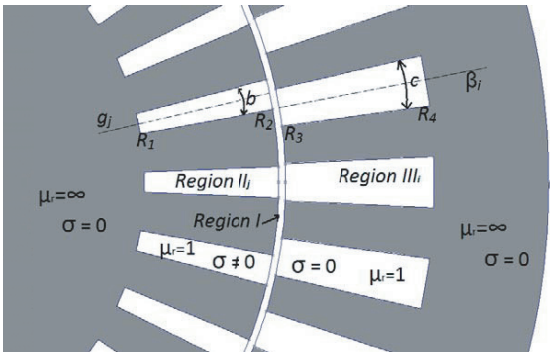

Figure 1. Studied multi-phases cage rotor induction machine.

1 The number of stator slots Q_s which is selected for having an integer number of slots per pole and per phase, and get the values close among all machines.

2 Opening angle slot (in degrees) is calculated from

$$c(n) = \frac{360}{Q_s(n)} \tag{1}$$

3 Number of turns per phase N_{ph} assumed to be equal to

$$N_{ph}(n) = \frac{3N_{ph}(3)}{n} \tag{2}$$

4 Number of conductors per stator slot N_c can be expressed as shown in

$$N_c(n) = \frac{2nN_{ph}(n)}{Q_s} \tag{3}$$

5 The stator slot area is given by

$$S(n) = \frac{N_c(n)}{N_c(3)} S(3) \tag{4}$$

6 External radius of stator slot

$$R_4(n) = \sqrt{2S(n)c(n) + R_3^2} \tag{5}$$

Table 1. Design details of the five studied machines.

Parameters	Symbol	Unit	3-ph	5-ph	7-ph	9-ph	11-p
Number of pole pairs	$\mathbf{p}$	-	2	2	2	2	2
Number of stator slots per pole per phase	$\mathbf{q}$	-	3	2	2	1	1
Number of stator slots	$\mathbf{Q_s}$	-	36	40	56	36	44
Number of turns per phase	$\mathbf{N_{ph}}$	-	90	56	40	30	24
Number of conductors per stator slot	$\mathbf{N_c}$	-	15	14	10	15	12
Stator slot opening width	$\mathbf{c}$	deg	5	4.5	3.21	5	4
Radius of external stator surface	$\mathbf{R_{ext}}$	mm	100	100	100	100	100
External radius of stator slot	$\mathbf{R_4}$	mm	83	83.7	83.7	83	82.6
Internal radius of stator	$\mathbf{R_3}$	mm	61	61	61	61	61
Number of rotor slot	$\mathbf{Q_r}$	-	30	30	30	30	30
External radius of rotor slot	$\mathbf{R_2}$	mm	60	60	60	60	60
Internal radius of rotor slot	$\mathbf{R_1}$	mm	40	40	40	40	40
Rotor slot opening width	$\mathbf{b}$	deg	4.2	4.2	4.2	4.2	4.2
Stack length	$\mathbf{L_u}$	mm	200	200	200	200	200
Conductivity of rotor bars	σ	MS/m	36	35	35	35	35
Peak phase current	$\mathbf{I_m}$	A	20	20	20	20	20
Peak phase voltage	$\mathbf{V_m}$	V	175	105	75	58.3	47.7

2.2. Magnetic Field Equations

The analytical model is formulated in complex vector potential and two-dimensional polar coordinates with the following assumptions.

- The stator and rotor core are assumed to be infinitely permeable with zero electrical conductivities;
- All multi-phases machines are supplied with a balanced n-phases sinusoidal currents or a balanced n-phases sinusoidal voltage;
- The time variation of the magnetic field is assumed to be sinusoidal;
- The resistance of the end-rings connecting the rotor bars are not considered; The current density in the stator slots has only one component along the z-axis;
- The stator and rotor slots are open and have radial sides without semi-closed slots, as shown in Fig. 1.

The general partial differential equation issued from Maxwell's equations in a continuous region in term of vector potential A, which has one component in z-axis and independent of z, can be expressed by [7] as

$$-\Delta\, A_z(r,\theta,t) = \mu_0\mu_r J_s(r,\theta,t) - \mu_0\mu_r\sigma\left(\frac{\partial\, A_z(r,\theta,t)}{\partial t} + \Omega\frac{\partial\, A_z(r,\theta,t)}{\partial\theta}\right) \tag{6}$$

In static analysis of induction motors, the first harmonic of the magnetic potential is considered dominant, and the relative movement between the stator and the rotor is represented by relative time

pulsation. Therefore, we assume that the pulsation of the potential vector is ω in the air-gap/stator regions and ω_{rm} in the rotor regions by mean of speed addiction

$$\omega_{rm} = s\omega = \omega - p\Omega$$

where s is the slip, p the number of pole pairs, and Ω the constant angular velocity of rotor.

From the preceding considerations, Eq. (6) becomes

$$-\Delta\ A_z(r,\theta,t) = \mu_0\mu_r J_s(r,\theta,t) - \mu_0\mu_r\sigma\frac{\partial\ A_z(r,\theta,t)}{\partial t} \tag{7}$$

and

$$A_z(r,\theta,t)\ =\ \Re e\{A_z(r,\theta)\ e^{j\omega t}\} \tag{8}$$

$$J_s(r,\theta,t)\ =\ \Re e\{J_s(r,\theta)\ e^{j\omega t}\} \tag{9}$$

in the air-gap and stator (i.e., Regions I, III)

$$A_z(r,\theta,t) = \Re e\{A_z(r,\theta)\ e^{j\omega_{rm}t}\} \tag{10}$$

in the rotor (i.e., Regions II).

From Eqs. (7) to (10), the magnetic vector potential $A(r,\theta)$ in each region is given by

$$\Delta A_z(r,\theta)\ =\ 0 \qquad In\ Regions\ I \tag{11}$$

$$\Delta A_z(r,\theta)\ =\ j\mu_0\mu_r\sigma\omega_{rm}A_z(r,\theta) \qquad In\ Regions\ II \tag{12}$$

$$\Delta A_z(r,\theta)\ =\ -\mu_0 J_s(r,\theta) \qquad In\ Regions\ III \tag{13}$$

where $J_s(r,\theta) = J_i$ is the stator slots current density, which is constant in each slot, σ the electrical conductivity of the rotor bars, $\mu_r = 1$ the relative permeability of the rotor bars, $j = \sqrt{-1}$ the complex number, and μ_0 the permeability of vacuum.

The field vectors $\overrightarrow{B}$ and $\overrightarrow{H}$, in the various regions, are coupled by

$$\overrightarrow{B}(r,\theta) = \mu\overrightarrow{H}(r,\theta) \tag{14}$$

The radial and tangential components of the magnetic flux density are deduced from $A(r,\theta)$ [10].

3. MAGNETIC FIELD SOLUTION

Using the Fourier series analysis and the method of separation variables, the solution of Eqs. (11)–(13) leads to determining the magnetic field distribution in all regions.

3.1. Solution of Laplace's Equation in the Air-Gap

In Region I, which is located between the radii R_2 and R_3 in Fig. 1, the solution of complex Laplace's Equation (11) is

$$A_{zI}(r,\theta) = A_{10} + A_{20}\ln(r) + \sum_{k=1}^{\infty}\left(A_{1k}r^k + A_{2k}r^{-k}\right)\sin(k\theta) + \sum_{k=1}^{\infty}\left(A_{3k}r^k + A_{4k}r^{-k}\right)\cos(k\theta) \tag{15}$$

where k is the spatial harmonic orders, and $A_{10} - A_{4k}$ are complex integration constants in Region I. This general solution accounts for the periodic boundary condition between 0 and 2π considering all types of multi-phase/multi-poles windings.

3.2. Solution of Helmholtz's Equation in the Rotor Bars

The jth rotor bar (i.e., Region II) is a slot with the classical boundary conditions shown in Fig. 2(a). The solution of the complex Helmholtz's Equation (12) is given by [8]

$$A_{zII_j}(r,\theta) = \sum_{m=0}^{\infty} B_{jm}g_m(r)\cos\left(\frac{m\pi}{b}\left(\theta - g_j + \frac{b}{2}\right)\right) \tag{16}$$

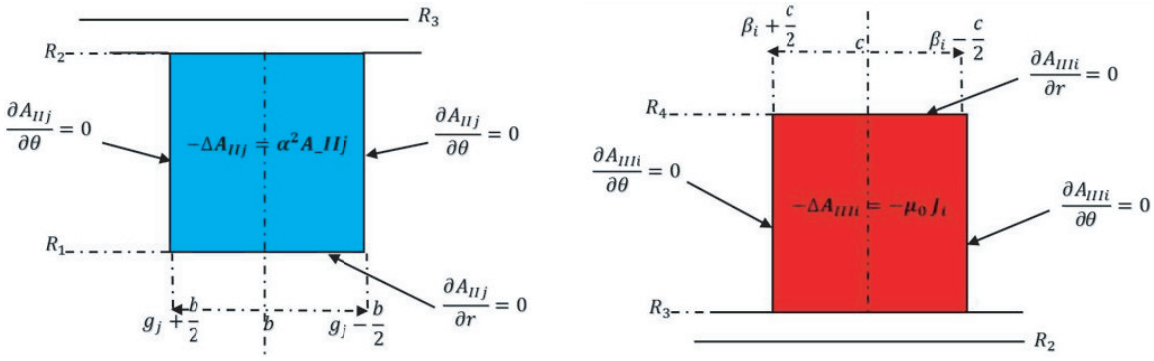

Figure 2. The boundary conditions of (a) rotor and (b) stator slots regions.

where B_{jm} are complex integration constants, and m is the spatial harmonic orders. For a Q_r rotor bars, j varies from 1 to Q_r and g_j is the angular position of the jth rotor bar and b the bar opening in radians. The expressions of $g_m(r)$ depend on the expression of α.

For $\alpha = (-j\omega_{rm}\sigma\mu_0)^{\frac{1}{2}}$

$$g_m(r) = J_{\frac{m\pi}{b}}(\alpha r) - \frac{J_{\frac{m\pi+b}{b}}(\alpha R_1)\alpha b R_1 - m\pi J_{\frac{m\pi}{b}}(\alpha R_1)}{Y_{\frac{m\pi+b}{b}}(\alpha R_1)\alpha b R_1 - m\pi Y_{\frac{m\pi}{b}}(\alpha R_1)} Y_{\frac{m\pi}{b}}(\alpha r)$$

For $\alpha = (j\omega_{rm}\sigma\mu_0)^{\frac{1}{2}}$

$$g_m(r) = I_{\frac{m\pi}{b}}(\alpha r) - \frac{I_{\frac{m\pi+b}{b}}(\alpha R_1)\alpha b R_1 + m\pi I_{\frac{m\pi}{b}}(\alpha R_1)}{-K_{\frac{m\pi+b}{b}}(\alpha R_1)\alpha b R_1 + m\pi K_{\frac{m\pi}{b}}(\alpha R_1)} K_{\frac{m\pi}{b}}(\alpha r)$$

where $J_{\frac{m\pi}{b}}(\alpha r)$, $Y_{\frac{m\pi}{b}}(\alpha r)$, $I_{\frac{m\pi}{b}}(\alpha r)$ and $K_{\frac{m\pi}{b}}(\alpha r)$ are the Bessel and modified Bessel functions of the first and second kinds of the order $\frac{m\pi}{b}$.

3.3. Solution of Poisson's Equation in the Stator Slots

The magnetic field in the stator slots is calculated analytically by solving Poisson's Equation (8). The solution of Eq. (13) in the ith slot subject to the boundary conditions shown in Fig. 2(b) is given by

$$A_{zIII_i}(r,\theta) = C_{i0} + \frac{1}{2}\mu_0 J_i R_4^2 \ln(r) - \frac{1}{2}\mu_0 J_i r^2 + \sum_{l=1}^{\infty} C_{il} h_l(r) \cos\left(\frac{l\pi}{c}\left(\theta - \beta_i + \frac{c}{2}\right)\right) \tag{17}$$

$$h_l(r) = r^{\frac{-l\pi}{c}} + R_4^{-2\frac{l\pi}{c}} r^{\frac{l\pi}{c}}$$

where $C_{i0} - C_{il}$ are complex integration constants and l is the spatial harmonic orders.

3.4. Interfaces Conditions

To determine Fourier series unknown constants, $A_{10} - A_{4n}$, $B_{j0} - B_{Q_rM}$ and $C_{i0} - C_{Q_sL}$ of magnetic field solutions in all regions, interfaces conditions should be introduced.

The interface conditions between Regions I and II at R_2 are

$$Az_I(R_2,\theta) = Az_{II}(R_2,\theta) \tag{18}$$

$$H_I(R_2,\theta) = H_{II}(R_2,\theta) \tag{19}$$

The interface conditions between Regions I and III at R_3 are

$$Az_{II}(R_3,\theta) = Az_{III}(R_3,\theta) \tag{20}$$

$$H_{II}(R_3,\theta) = H_{III}(R_3,\theta) \tag{21}$$

The preceding four interface conditions permit to determine a linear system of equations which depend on the harmonic orders (k, m, and l) choice in each region. Some details of the development of interface conditions can be found in [8] and [10].

3.5. Broken Bars Condition

The broken rotor bars are represented by Region II_d having an electrical conductivity equal to zero. The resistance of rotor bars is infinity in this case and the eddy current is null.

The solution of Equation (12) becomes

$$\begin{aligned} A_{zII_{jd}}(r,\theta) &= B_{j0} + \sum_{m=1}^{\infty} B_{jm} h_m(r) \cos\left(\frac{m\pi}{b}\left(\theta - g_i + \frac{b}{2}\right)\right) \\ h_m(r) &= r^{\frac{-m\pi}{b}} + R_1^{-2\frac{m\pi}{b}} r^{\frac{m\pi}{b}} \end{aligned} \tag{22}$$

3.6. Rotor Bar Current and Winding Definition

The eddy-current density induced in the jth rotor bar is given by

$$J_{bj}(r,\theta) = -j\omega_{rm}\sigma_j A_{zIIj}(r,\theta) \tag{23}$$

The current in the jth rotor bar is

$$Ib_j = \int_{R_1}^{R_2} \int_{g_j-\frac{b}{2}}^{g_j+\frac{b}{2}} J_{bj}(r,\theta) dr d\theta \tag{24}$$

It should be noticed that in the broken bars, the electrical conductivity is null, and the current density is zero.

The stator current density in the slots for multi-phase single layer winding is defined by a connection matrix between phase currents and stator slots as (for one pole)

$$C = \begin{array}{c} \overbrace{}^{i} \\ 1 \\ 2 \\ \vdots \\ \frac{n+1}{2} \\ \frac{n+3}{2} \\ \vdots \\ n \end{array} \begin{bmatrix} \overbrace{1..1}^{1:q} & \overbrace{0..0}^{q+1:2q} & \overbrace{0..0}^{2q+1:3q} & \dots & \overbrace{0..0}^{(n-2)q+1:(n-1)q} & \overbrace{0..0}^{(n-1)q+1:nq} \\ 0..0 & 0..0 & 1..1 & \dots & 0..0 & 0..0 \\ \vdots & \vdots & \vdots & \ddots & \vdots & \vdots \\ 0..0 & 0..0 & 0..0 & \dots & 0..0 & 1..1 \\ 0..0 & -1..-1 & 0..0 & \dots & 0..0 & 0..0 \\ \vdots & \vdots & \vdots & \ddots & \vdots & \vdots \\ 0..0 & 0..0 & 0..0 & \dots & -1..-1 & 0..0 \end{bmatrix} \tag{25}$$

where n is the number of phases and q the number of slots per pole and per phase.

It is important to notice that the proposed analytical model can be easily extended to double layer winding.

For n-phase induction motors supplied by balanced sinusoidal current, stator current vector is defined as

$$I_s = I_m \left[1 \; e^{-j\frac{2\pi}{n}} \; \dots \; e^{-j\frac{2(n-1)\pi}{n}}\right]$$

Notice that in the open phase condition the current of phases is zero, and the current vector will be.

$$I_s = I_m \left[1 \; e^{-j\frac{2\pi}{n}} \; \dots \; \overbrace{0}^{ph_{Open}} \; \dots \; e^{-j\frac{2(n-1)\pi}{n}}\right]$$

The current-density in stator slots is

$$J_i = \frac{N_c}{S}[I_s] \cdot [C] \tag{26}$$

where S is the surface of the stator slots and N_c the number of conductors in the slot.

4. CIRCUIT MODEL PARAMETERS IDENTIFICATION, STATOR CURRENT, TORQUE, AND RADIAL FORCES

The determination of the fluxes permits the calculation of lumped parameters of the equivalent circuit of induction motor. Neglecting the iron losses and assuming the first harmonic hypothesis, the EEC shown in Fig. 3 can be considered.

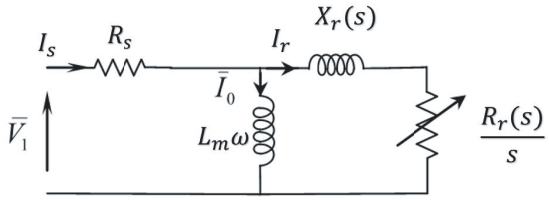

Figure 3. EEC of one phase for the cage rotor multi-phases induction motors.

In this circuit, the flux leakage inductance is lumped in the secondary branch. The electrical components of the circuit are defined by:

1) R_s is the stator resistance which can be determined by classical analytical formula;
2) L_m is the stator inductance (i.e., the magnetizing inductance);
3) $X_r(s)$ is the leakage inductance expressed in the rotor frame which depends on the slip;
4) $R_r(s)$ is the equivalent resistance expressed in the rotor frame which depends on the slip.

The magnetizing inductance L_{m_i} can be determined by performing a simulation of no-load operation (i.e., $s = 0$). With an input n-phase currents, the resolution of the field equations allow determining the magnetic flux vector $\Psi = [\psi_1 \dots \psi_n]$. So we have.

$$L_{m_i} = \psi_i / I_{s_i}$$

The complex phases flux vector is given by

$$\Psi = N_c \left[\phi_1 \dots \phi_{Q_s}\right] \cdot [C]^T \tag{27}$$

where the flux linkage is calculated from the method based on Stokes theorem using the vector potential in the stator slots

$$\phi_i = \frac{L_u}{S} \int_{R_3}^{R_4} \int_{\beta_i - \frac{c}{2}}^{\beta_i + \frac{c}{2}} A_{zIII_i}(r,\theta) r dr d\theta \tag{28}$$

where $A_{zIII_i}(r,\theta)$ is the vector potential given by (14).

The calculation of the rotor parameters needs the simulation of the electromagnetic behavior for a given value of the slip $s \neq 0$. For load operation, an input phase current is imposed. The resolution of the field equation allows determining the magnetic fluxes. Then, the secondary current I_r is determined for each phase by

$$I_{r_i}(s) = I_{s_i} - \psi_i / L_{m_i} \tag{29}$$

The secondary impedance $Z_{r_i}(s)$ can be calculated for each phase by

$$\begin{aligned} Z_{r_i}(s) &= j\omega\psi_i / I_{r_i}(s) \\ R_{r_i}(s) &= s\, \Re e\{Z_{r_i}(s)\} \\ X_{r_i}(s) &= \Im m\{Z_{r_i}(s)\} \end{aligned} \tag{30}$$

This approach is adopted for the calculation of the EEC parameters by using both FEM and analytical model presented in this paper. When the machine is fed with a constant n-phases voltage $V_s = V_m[1\ e^{-j\frac{2\pi}{n}}\ \dots\ e^{-j\frac{2(n-1)\pi}{n}}]$ the stator current for each slip can be determined for by the EEC as

$$I_{s_i}(s) = V_{s_i} / (R_{s_i} + (Z_{r_i}(s) // L_{m_i}\omega)) \tag{31}$$

In healthy condition the EEC parameters are the same for all phases, although in the case of broken bars or open phase's conditions, the EEC parameters are different between the phases, which induce different phases current. The torque-slip characteristic can be obtained analytically and by FEM. Of course, for a given stator current at a given slip, the torque is calculated by the Maxwell stress tensor method in Eq. (33). The electromagnetic torque can also be determined using the EEC as

$$T_{em} = \frac{P_{tr(s)}}{\frac{\omega}{p}} \tag{32}$$

where $P_{tr(s)}$ is the active power transformed to rotor.

According to the Maxwell stress tensor method, the electromagnetic torque T_{em} is computed using the analytical expression

$$T_em = \frac{L_u R_g^2}{\mu_0} \int_0^{2\pi} \frac{1}{2} \Re e\{B_{Ir}(R_g,\theta) \cdot B^*_{I\theta}(R_g,\theta)\} d\theta \tag{33}$$

where R_g is the radius of a circle placed at the middle of the air-gap, L_u the axial length of the motor, and $B_{Ir}(R_g,\theta)$ and $B^*_{I\theta}(R_g,\theta)$ are, respectively, the radial and tangential components of the flux density in the middle of air gap.

The radial and tangential-components of magnetic pressure in function of the spatial angle of the machine θ in the middle of air gap for giving slip s are defined as [11].

$$P_r(s,\theta) = \frac{1}{2\mu_0}\left(B_{Ir}(R_g,\theta)^2 - B_{I\theta}(R_g,\theta)^2\right) \tag{34}$$

$$P_\theta(s,\theta) = \frac{1}{\mu_0} B_{Ir}(R_g,\theta) \cdot B_{I\theta}(R_g,\theta) \tag{35}$$

The x- and y-components of the radial force for giving slip are calculated as

$$F_x(s) = R_g L_u \int_0^{2\pi} [P_r \cdot \cos(\theta) - P_\theta \cdot \sin(\theta)] d\theta \tag{36}$$

$$F_y(s) = R_g L_u \int_0^{2\pi} [P_r \cdot \sin(\theta) + P_\theta \cdot \cos(\theta)] d\theta \tag{37}$$

The radial force magnitude is

$$F_r(s) = \sqrt{F_x^2 + F_y^2} \tag{38}$$

Notice that in the healthy bars conditions, the radial force is null because of the symmetry of magnetic pressure created in each pole, but when ones of rotor bars broken, this pressure will be non-symmetric and a radial force will appear.

5. RESULTS AND VALIDATION

In this section, the 5-phase machine is taken as reference to validate the analytical model. All results are verified by FEM [14].

5.1. No-Load Condition with Current Supply

Under no-load condition (i.e., $s = 0.0001$), Fig. 4 shows the flux lines in the 5-phase machine obtained with FEM. The radial and tangential components of the flux density distribution in the middle of the air-gap are shown in Fig. 5. A very good agreement can be seen between the numerical and analytical results.

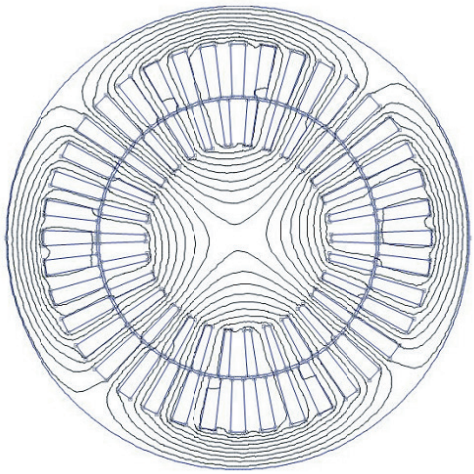

Figure 4. Flux lines for 5-phase machine at no-load condition (i.e., $s = 0.0001$) obtained with FEM.

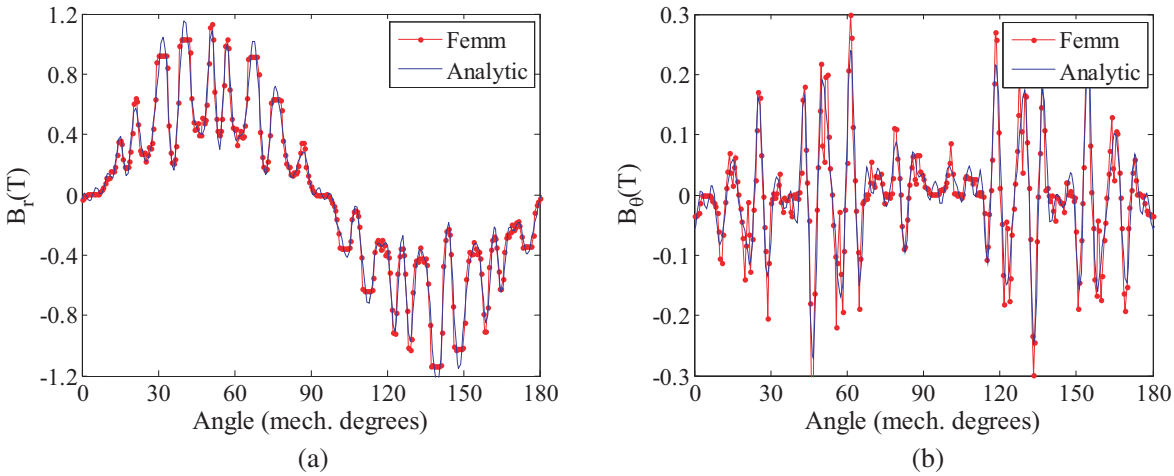

Figure 5. (a) Radial and (b) tangential components of the flux density in the middle of the air-gap for 5-phase machine and no-load condition (i.e., $s = 0.0001$).

5.2. Locked-Rotor Condition with Current Supply

The flux lines, the real part of eddy-current density distribution in the middle of the rotor bar No. 8 and the real part of the current in each rotor bars are shown in Fig. 6. The radial and tangential flux density waveform in the middle of the air-gap is shown in Fig. 7. Compared with the no-load results, one can observe the influence of the eddy-currents on both the radial and the tangential flux densities. It can be seen that the radial component of the flux density decreases.

5.3. Circuit Model Parameters, Stator Current, and Torque

The values of the self-inductances calculated by FEM at $s = 0.0001$ for the 5-phase machine is $L_m\omega = 7.48$ while the analytical model gives $L_m\omega = 7.49$. Fig. 8 shows the evolution of parameters R_r and X_r versus the slip. There is a good agreement between analytic and FEM results.

The comparison of FEM, circuit model, and analytical calculation of the current-slip and torque-slip characteristics under constant voltage are shown in Fig. 9. It can be seen that the results obtained analytically are in good agreement with FEM.

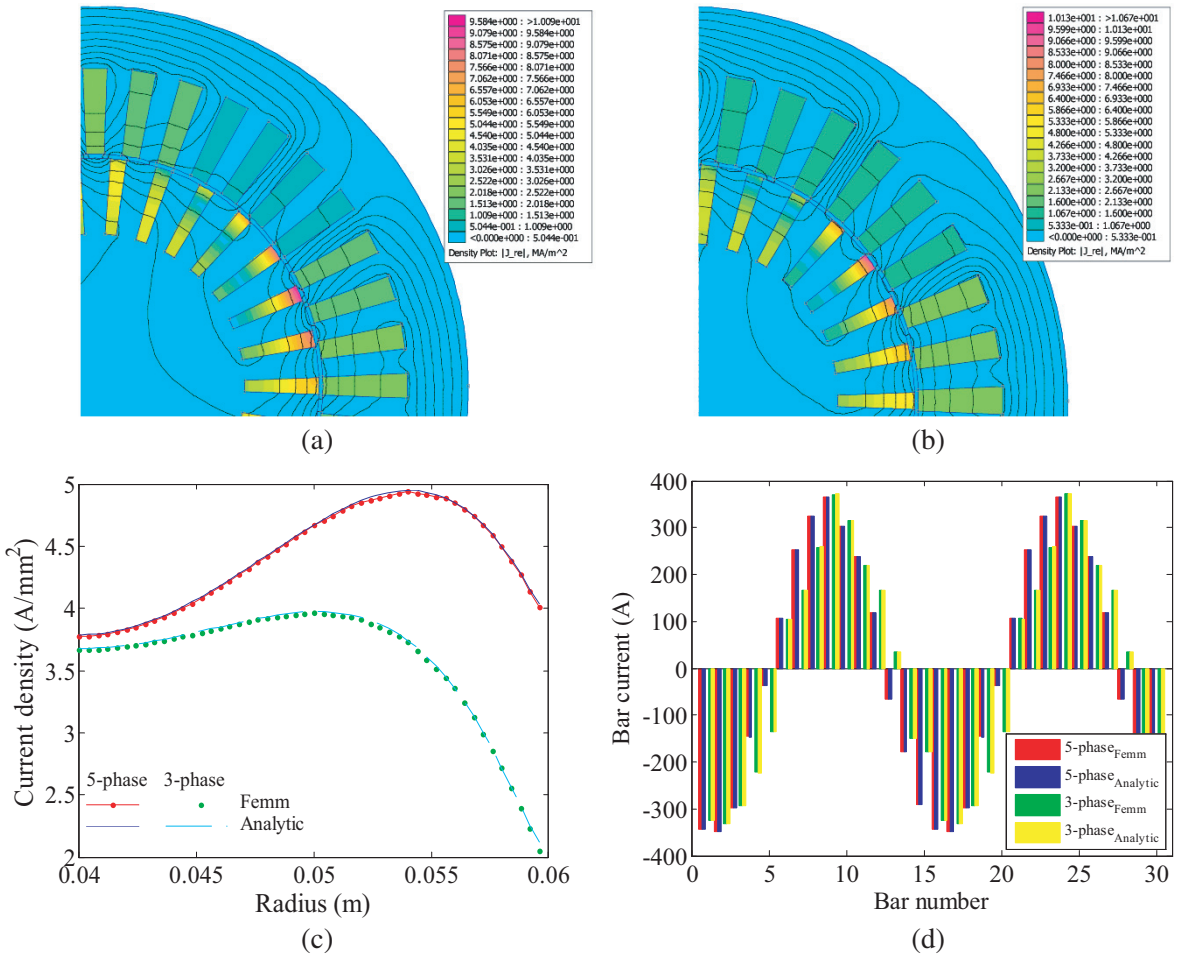

Figure 6. (a) Flux lines for 5-phase machine, (b) flux lines for 3-phase machine, (c) real part of eddy-current density distribution (A/mm^2), and (d) the current in the rotor bars for 5-phase and 3-phase machines at locked rotor condition (i.e., $s = 1$).

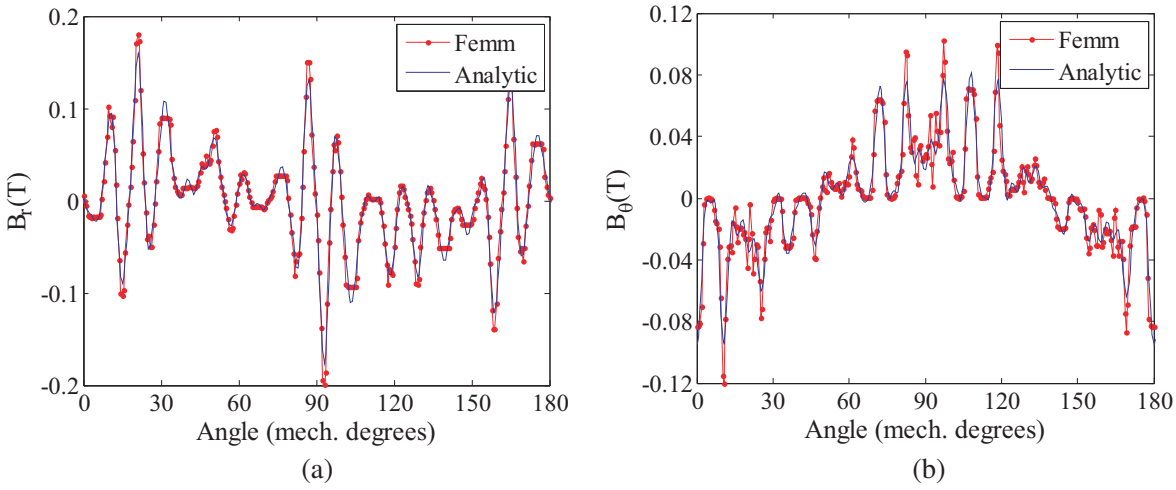

Figure 7. (a) Radial and (b) tangential components of the flux density in the middle of the air-gap for 5-phase machine and locked rotor condition (i.e., $s = 1$).

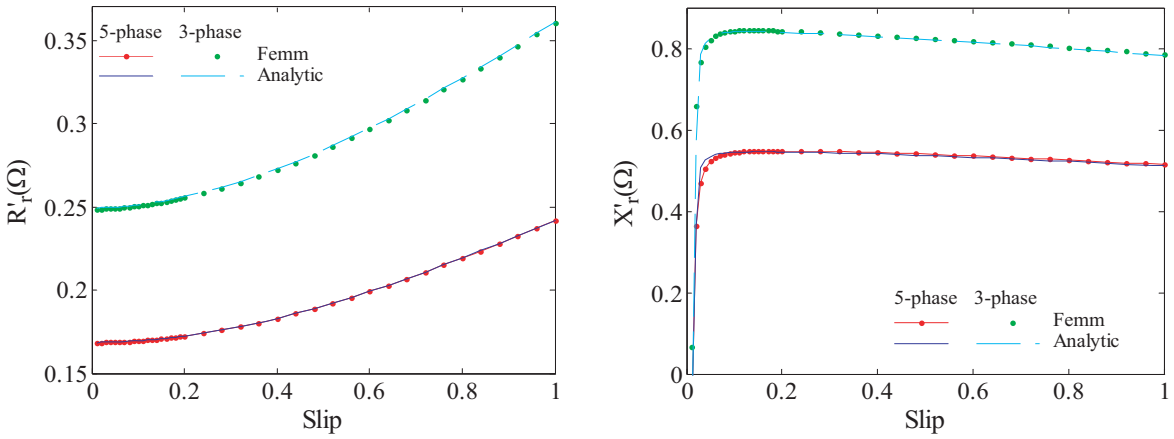

Figure 8. Comparison between analytical and finite element circuit model rotor parameters versus slip for 5-phase and 3-phase machines.

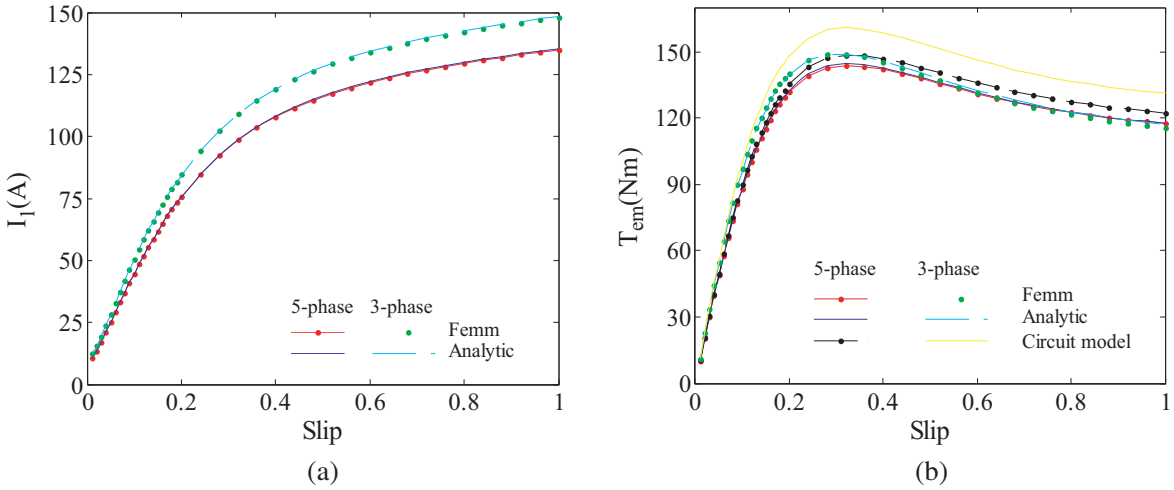

Figure 9. (a) Current-slip and (b) torque-slip characteristics for 5-phase and 3-phase machines under constant balanced voltage.

5.4. Magnetic Field and Eddy-Current On-Load at $s = 0.02$

Under constant voltage, on-load flux lines and current in each rotor bars at $s = 0.02$ are shown in Fig. 10. The corresponding radial and tangential flux density waveforms in the middle of the air-gap are shown in Fig. 11. A very good agreement can be seen between the numerical and analytical results.

5.5. Broken Bars Condition

In this section, the bars Nos. 9 and 10 are supposed broken as a machine fed with a balanced constant voltage, the stator currents are not balanced (Fig. 13(a)). The flux lines, eddy-current density distribution and the current in the rotor bars are shown in Fig. 12 in the case of bars being broken (i.e., $\sigma_9 = \sigma_{10} = 0$). Fig. 13 shows the stator current, electromagnetic torque, and created unbalanced radial force versus slip.

A comparison between one broken bar and two broken bars is shown in Fig. 14. One can see that the influence of broken bars has been affected the torque and create unbalanced force.

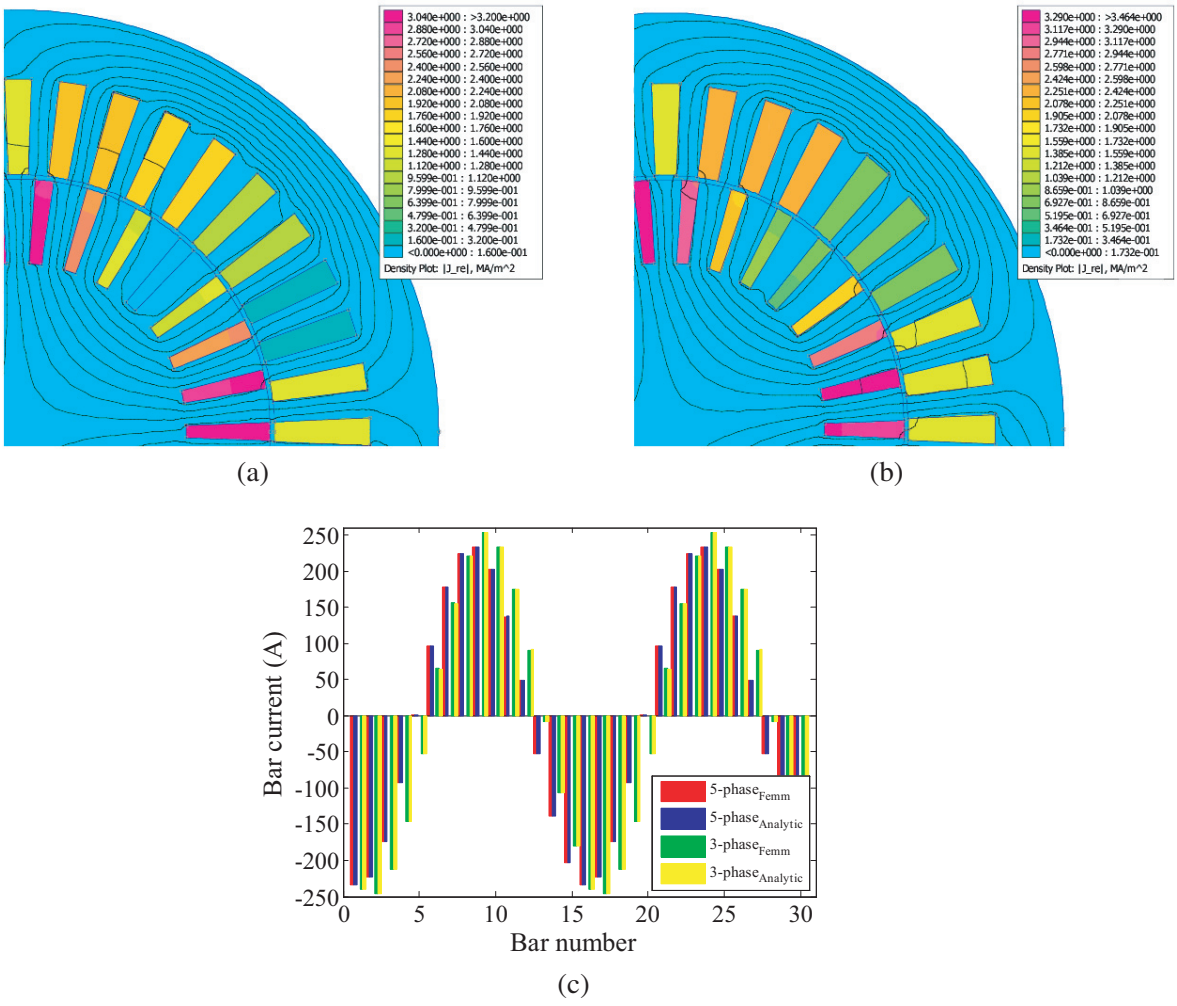

Figure 10. (a) Flux lines for 5-phase machine, (b) flux lines for 3-phase machine, and (c) the current in the rotor bars for 5-phase and 3-phase motors on-load at $s = 0.02$.

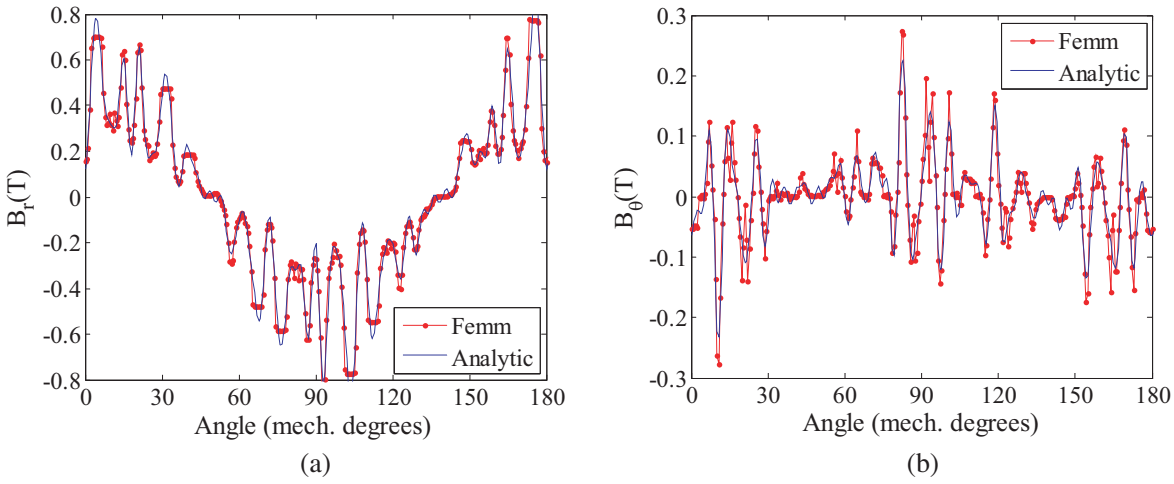

Figure 11. (a) Radial and (b) tangential components of the flux density in the middle of the air-gap for 5-phase machine on-load at $s = 0.02$.

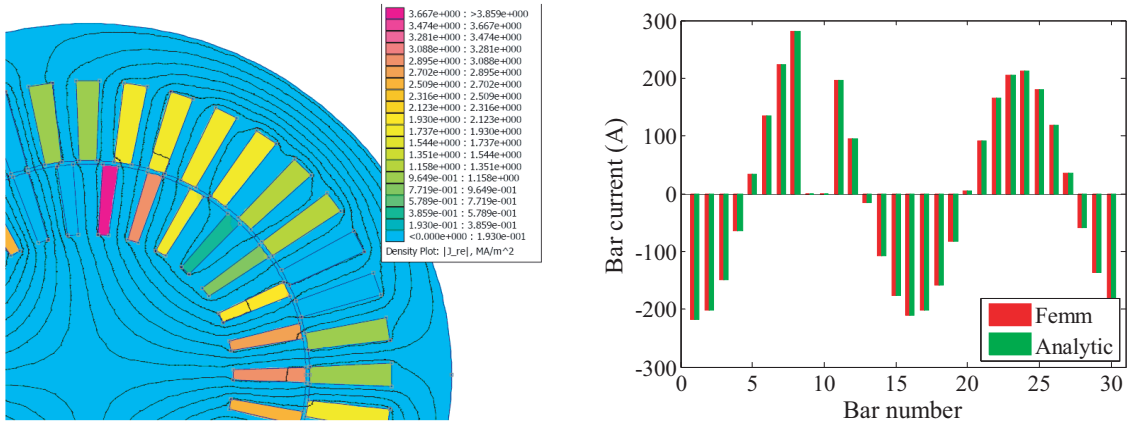

Figure 12. (a) Flux lines, and (b) the current in the rotor bars for 5-phase machine on-load at $s = 0.02$ and bars 9 and 10 broken.

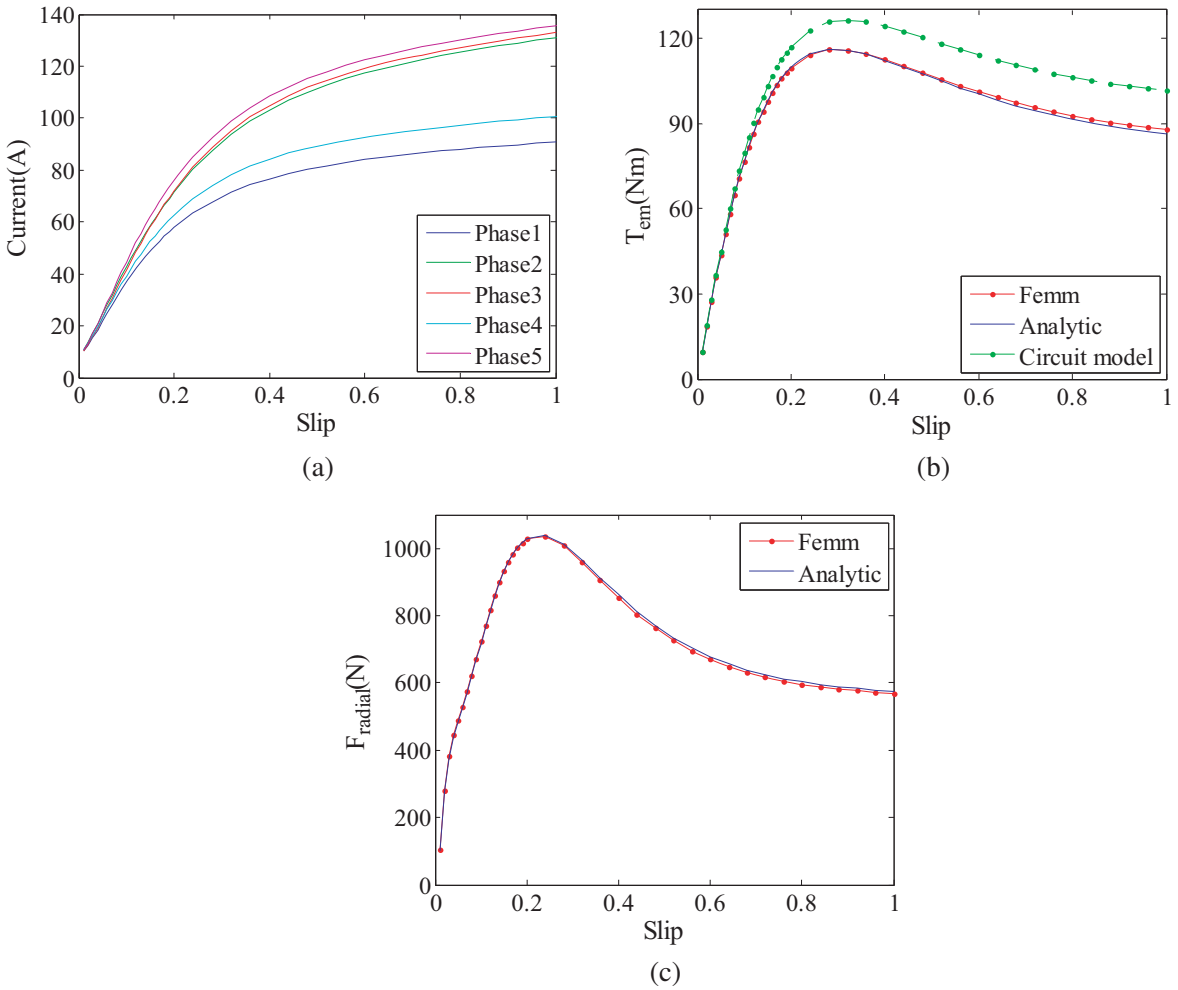

Figure 13. (a) Phases currents, (b) electromagnetic Torque, and (c) radial force versus slip for 5-phase machine and two broken bars condition.

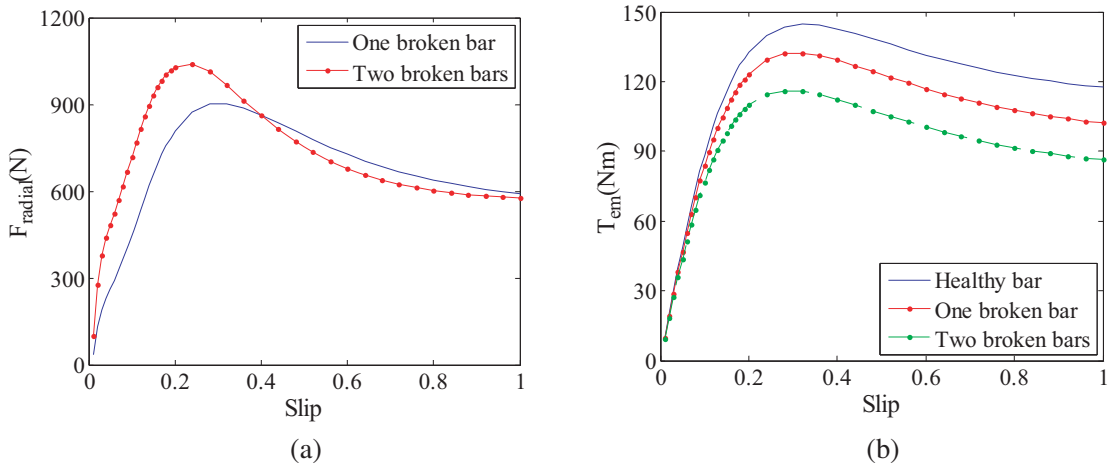

Figure 14. Comparison between (a) radial force, (b) Torque versus slip characteristic for 5-phase machine in healthy, one broken bar, and two broken bars conditions.

5.6. Open Phases Condition

In this section, the phases Nos. 1 and 2 are supposed open; therefore, their currents are null (Fig. 16). The flux lines, eddy-current density distribution and the current in the rotor bars are shown in Fig. 15 in the case of 2 phases open (i.e., $I_1 = I_2 = 0$). Fig. 16 shows the stator current, the electromagnetic torque versus slip. A comparison between one phase and two phases open are shown in Fig. 16(c). One can see that the influence of open phases which has affected the torque.

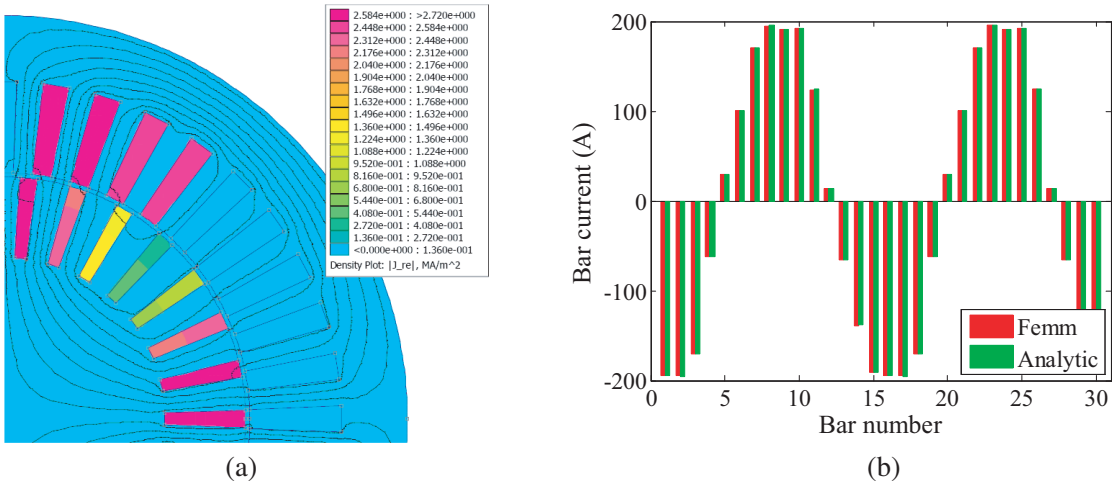

Figure 15. (a) Flux lines, and (b) the current in the rotor bars for 5-phase machine on-load at $s = 0.02$ and phases 1 and 2 open.

6. INFLUENCE OF NUMBER OF PHASE IN BROKEN BARS AND OPEN PHASES CONDITIONS

In this section, a comparative study using the analytic model among all polyphase induction machines in several states is presented. This study allows showing how the number of phases influences in the fault case of polyphase machines in the rotor or in the stator. In healthy case (Fig. 17) all machines have close characteristics for nominal running. The 11-phase machine has a more important maximum,

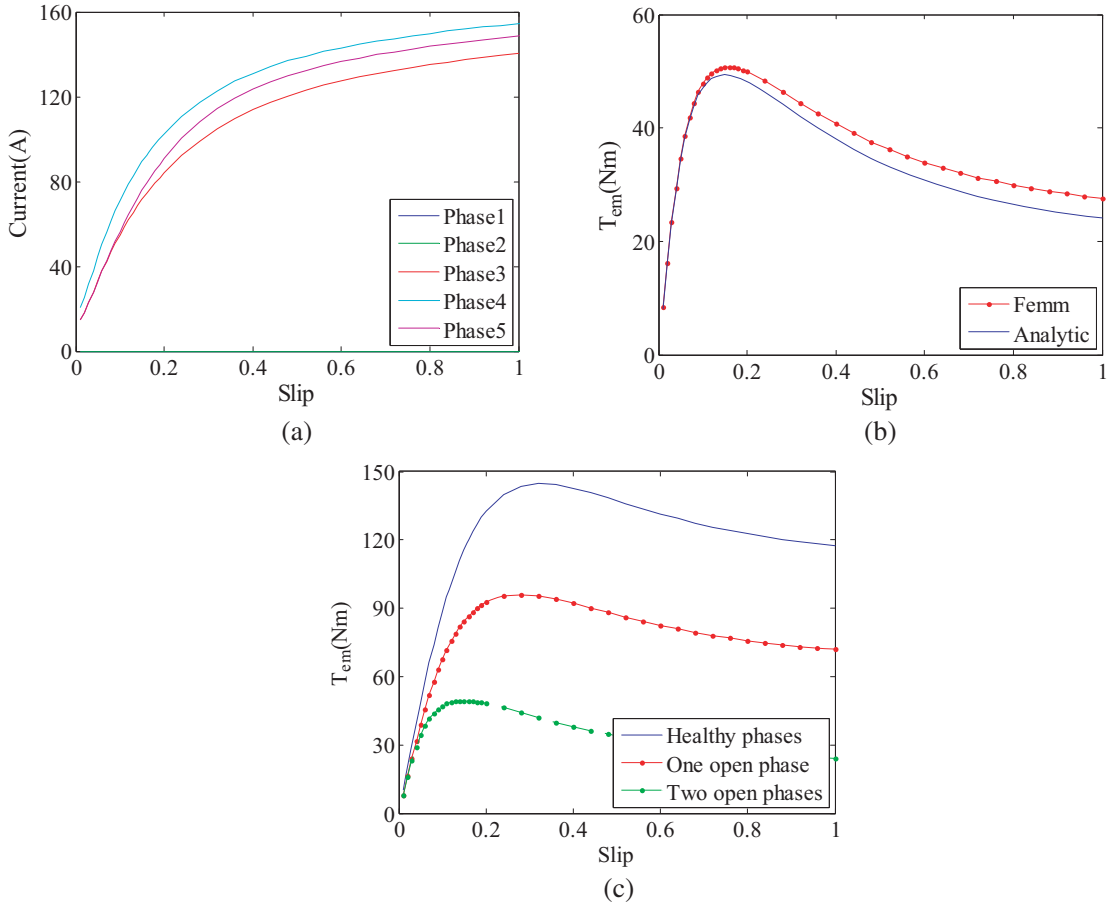

Figure 16. (a) Phases currents, and (b)–(c) electromagnetic Torque versus slip for open phases condition in 5-phase machine.

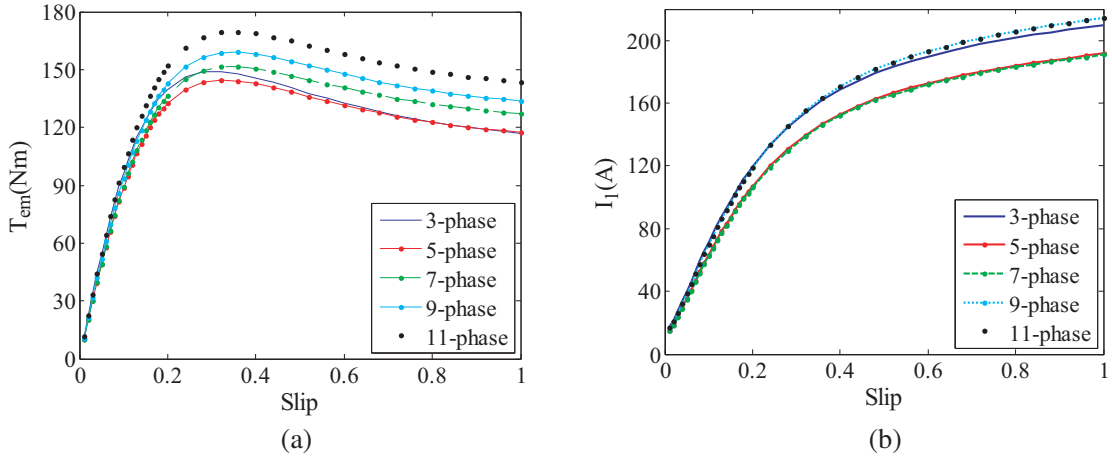

Figure 17. (a) Electromagnetic Torque, (b) stator current versus slip in healthy case.

and start-up torque, and the same observation is noticed for stator currents.

Figure 18 shows torque versus slip characteristics for broken bars conditions. The electromagnetic torque is not highly affected for nominal running, although the maximum and start-up torques decrease by 37.5% for 3-phase machine and only 17.24% for 11-phase machine.

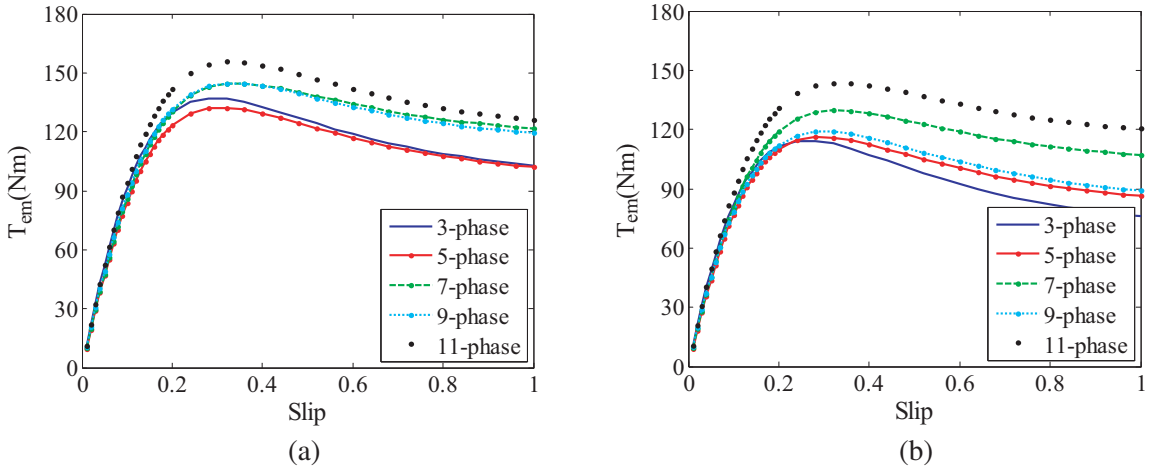

Figure 18. Electromagnetic Torque for (a) one broken bar, (b) two broken bars.

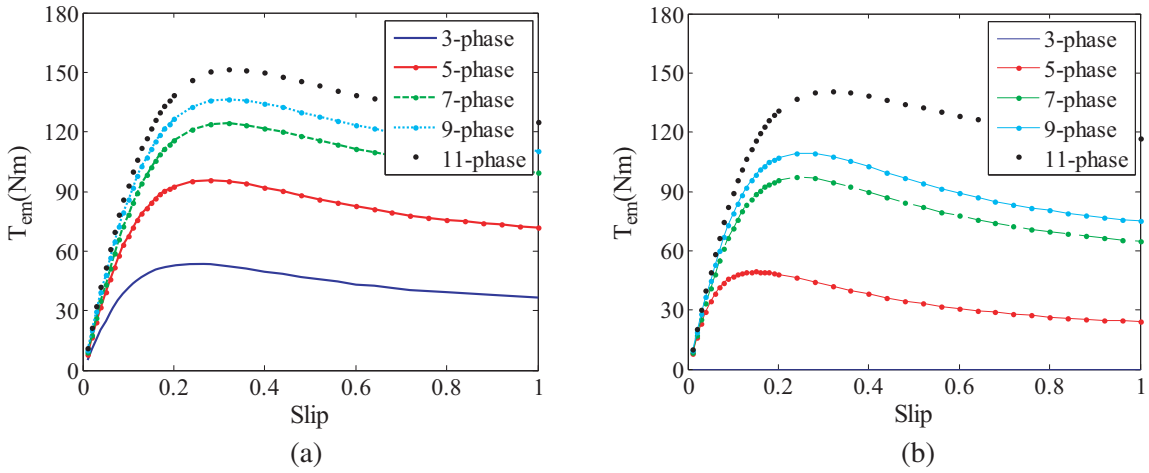

Figure 19. Electromagnetic Torque for (a) one open phase, (b) two open phases.

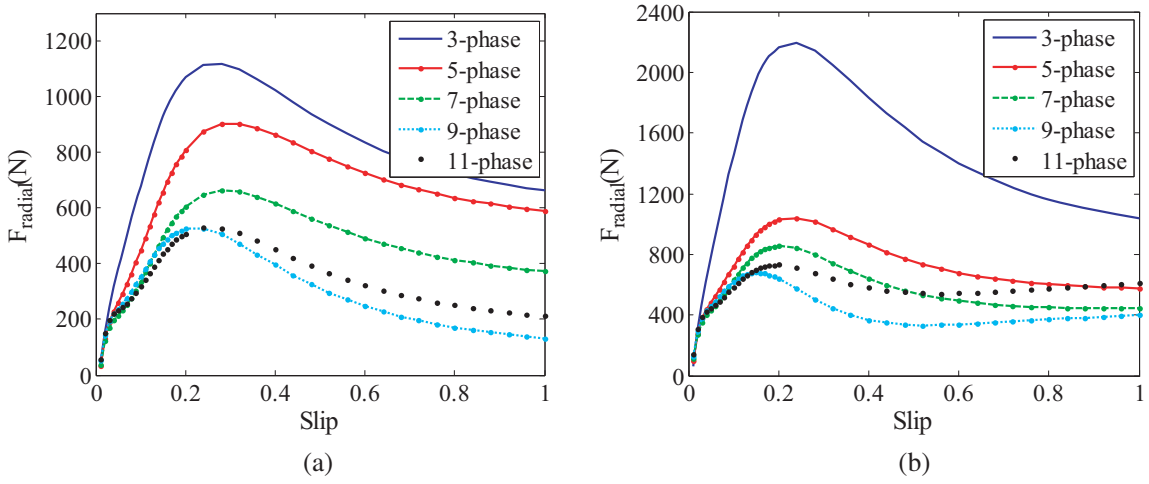

Figure 20. Radial force versus slip for (a) one broken bar, and (b) two broken bars conditions.

For the open phase's condition shown in Fig. 19, the torque is affected for all values of slip. This effect is reduced for higher number of phases' machine. For 11-phase machine, the torque decreases by 6% for nominal running and by 17% for start-up torque. Fig. 20 shows the radial force created by the broken of one of the rotor bars. For a slip smaller than 0.2, the 11-phase machine is the least affected.

7. CONCLUSION

In this paper, we propose an improved analytical method for predicting magnetic field distribution, electromagnetic performances and parameters of electrical equivalent circuit in healthy, broken bars, and open phase's conditions of cage rotor multi-phases induction motors. The presented analytical model based on subdomain method is used to determine analytical expressions of eddy current, electromagnetic torque, stator current and unbalanced magnetic force (UMF) in healthy, broken bars and open phase's conditions. Both cases are considered: the machine fed with sinusoidal current or voltage. Five identical powers rated machines are designed with analyzing the effect of a number of open phases and broken bars on electromagnetic torque, stator current and UMF. We have seen that the augmentation of number of phases reduces the radial force due to broken bars which is null in healthy case for any multi-phases machine. It is noticed that the start-up torque of the machine in broken bars or open phase's conditions is not highly affected for higher multi-phases machines which offer a greater security in several applications.

REFERENCES

1. Levi, E., "Multiphase electric machines for variable-speed applications," *IEEE Trans. Ind. Elec.*, Vol. 55, No. 5, 1893–1909, May 2008.
2. Pereira, L., A., Scharlau, C., C., Pereira, L., F., A., and Haffner, J., F., "General model of a five-phase induction machine allowing for harmonics in the air gap field," *IEEE Trans. Energy Conversion*, Vol. 21, No. 4, 891–899, December 2006.
3. Abdel-khalik, A. S., M. I. Masoud, A. Shehab, and A. M. Massoud, "Effect of current harmonic injection on constant rotor volume multiphase induction machine stators: A comparative study," *IEEE. Trans. Ind. Apps.*, Vol. 48, No. 6, 2002–2013, November–December 2012.
4. Matyas, A. R., K. A. Biro, and D. Fodorean, "Multi-phase synchronous motor solution for steering applications," *Progress In Electromagnetics Research*, Vol. 131, 63–80, September 2012.
5. Apsley, J. and S. Williamson, "Analysis of multiphase induction machines with winding faults," *IEEE Trans. Ind. Apps.*, Vol. 42, No. 2, 465–472, March–April 2006.
6. Vaseghi, B., N. Takorabet, and F. Meibody-Tabar, "Transient finite element analysis of induction machines with stator winding turn fault," *Progress In Electromagnetics Research*, Vol. 95, 1–18, 2009.
7. Mori, D. and T. Ishikawa, "Force and vibration analysis of induction motors," *IEEE Trans. on Magnetics*, Vol. 41, No. 5, 1948–1951, May 2005.
8. Boughrara, K., N. Takorabet, R. Ibtiouen, O. Touhami, and F. Dubas, "Analytical analysis of cage rotor induction motors in healthy, defective, and broken bars conditions," *IEEE Trans. on Magnetics*, Vol. 51, No. 2, 8200317–8200334, February 2015.
9. Lubin, T., S. Mezani, and A. Rezzoug, "Analytic calculation of eddy currents in the slots of electrical machines application to cage rotor induction motors," *IEEE Trans. on Magnetics*, Vol. 41, No. 11, 4650–4659, November 2011.
10. Boughrara, K., F. Dubas, and R. Ibtiouen, "2-D analytical prediction of eddy currents, circuit model parameters, and steady-state performances in solid rotor induction motors," *IEEE Trans. on Magnetics*, Vol. 50, No. 12, 7028214–7028228, December 2014.
11. Kim, D. Y., G. H. Nam, and G. H. Jang, "Reduction of magnetically induced vibration of a spoke-type IPM motor using magnetomechanical coupled analysis and optimization," *IEEE Trans. on Magnetics*, Vol. 49, No. 9, 5097–5105, September 2013.

12. Boutora, Y., N. Takorabet, and R. Ibtiouen, "Analytical model on real geometries of magnet bars of surface permanent magnet slotless machine," *Progress In Electromagnetics Research B*, Vol. 66, 31–47, 2016.
13. Pyrhonen, J., T. Jokinen, and V. Hrabovcova, *Design of Rotating Electrical Machines*, John Wiley & Sons, Ltd., 2008.
14. Meeker, D. C., *Finite Element Method Magnetics*, Version 4.2, April 1, 2009 Build, http://www.femm.info.